Journal of Sound and Vibration 330 (2011) 75–86

Contents lists available at ScienceDirect

Journal of Sound and Vibration

journal homepage: www.elsevier.com/locate/jsvi

A railway track dynamics model based on modal substructuring and a cyclic boundary condition

Luis Baeza [a,*], Huajiang Ouyang [b]

[a] Centro de Investigación en Tecnología de Vehículos, Departamento de Ingeniería Mecánica y de Materiales, Universidad Politécnica de Valencia, Camino de Vera s/n, 46022 Valencia, Spain

[b] Department of Engineering, University of Liverpool, Liverpool L69 3GH, United Kingdom

ARTICLE INFO

Article history:
Received 27 July 2009
Received in revised form
28 July 2010
Accepted 28 July 2010
Handling Editor: A.V. Metrikine
Available online 21 August 2010

ABSTRACT

This article presents a technique for modelling the coupled dynamics of a railway vehicle and the track. The method is especially useful for simulating the dynamics of high speed trains running on nonlinear tracks. The main hypothesis is a cyclic system: an infinite track on which there is an infinite set of identical vehicles spaced at a regular interval of distance. Thus the main problems of the finite-length track models (e.g. the waves that reflect at the end of the track and interact with the vehicle; and the time interval of integration must be shorter than the track length divided by the velocity) are avoided. The flexibility of the method can be observed from the case studies presented in the present work: a vehicle passing over a hanging sleeper, and the vehicle–track dynamics for different ballast compaction cases. The results show the influence of the hanging sleeper gap on the wheel–rail contact forces, and the bending moment at the sleeper for different ballast compaction cases.

1. Introduction

The coupled dynamic response of a railway vehicle and the track is of great practical interest to the industry. It is associated with some very important railway engineering problems such as wheelflats or other wheel tread irregularities (out of round wheels) [1], rail corrugation [2], rail head defects [3] and rolling noise [4]. In order to analyse these and other problems, many researchers have developed dynamic vehicle–track models and these models basically differ in how the track is treated. The track is a large system that can be considered as an infinite structure and it is made up of the ballast and elastomeric materials which have nonlinear behaviour. Due to these complex characteristics, models for only finite nonlinear or infinite linear track have been established and can be found in the literature.

A first approach of an infinite track consisted of a homogeneous track that was modelled as a Winkler beam. The infinite Euler beam on discrete elastic supports was analysed in [5] by means of Fourier series. A sophisticated homogeneous track model was developed in [6] for modelling a slab track with embedded rails. The slab was modelled as a Kirchhoff plate on an elastic foundation; the rails were Euler beams and were continuously supported on the slab. The wheel–rail contact force was supposed to be harmonic and the steady-state response was calculated. The solution was obtained by using the Fourier transform in the frequency and the wavenumber domains. A similar procedure was presented in references [7,8]. The first work [7] considered an infinite double beam system that modelled a rail on a continuous slab. The second article [8] led to a model of the track with discrete supports (sleepers). The rails (Euler beams) were periodically supported on

* Corresponding author. Tel.: +34 963877621; fax: +34 963877629.
E-mail address: lbaeza@mcm.upv.es (L. Baeza).

0022-460X/$ - see front matter © 2010 Elsevier Ltd. All rights reserved.
doi:10.1016/j.jsv.2010.07.023

rigid sleepers on an infinite elastic layer. The method presented in [9] studied vibration induced by traffic and modelled the infinite soil in the frequency-wavenumber domain through the boundary element method. Following a different approach, the periodicity condition and the time Fourier transformation were employed in order to study an infinite Euler beam on discrete elastic supports [10].

The U-transformation method was employed in [11] for modelling a beam on discrete rigid supports. The U-transformation uncoupled the equations of motion together with the boundary and continuity conditions for N periodic structures. The method led to an infinite track when N approaches infinity.

Another approach was based on Mead's works (e.g. [12]) which implemented a technique for analysing wave propagation in infinite periodic structures in order to model a railway track. Some researchers extended this approach to other railway applications: rolling noise [13,14]; corrugation problem [15]; the dynamic response of the vehicle to track irregularities [16].

Nonlinear models of wheel–rail contact or any other interfaces of the system have been studied with a finite track. Finite-length track models are characterised by the end-rail effects. Waves originating from the vehicle–track interaction get reflected at the end-track and interact with the vehicle if the distance from the vehicle to the rail-end is small. Therefore the distance between the vehicle and the rail-end must be sufficiently long to avoid wave reflection; and thus such track models need a large number of degrees of freedom.

The Finite Element Method (FEM) is one of the most versatile techniques and it has been implemented for modelling the complete track in [17,18]. The FEM is known to provide a large number of coordinates and it can be reduced through a modal approach [19,20] where a small number of vibration modes are retained in the dynamic analysis. The paper presented in [21] led to a reduction of the computational cost through a substructuring technique where the rail vibration was described by a modal approach. The mode shapes of the rail were used to describe the deformed rail and its dynamic response and they were obtained from the free–free boundary conditions. The high-frequency dynamics of the track (400 Hz to 1.5 kHz) can be modelled properly through a Winkler beam [4], in which case the mode shapes of the real rail are very similar to those of a free–free beam. Consequently, the number of modes of the rail (and modal coordinates) necessary for simulating the behaviour of the track below 1.5 kHz is reduced.

The present work presents a method for simulating the dynamic interaction of a railway vehicle and the track. It adopts an infinite cyclic track–train system on which an infinite set of identical vehicles are operating and the rail is represented by a modal approach. The rail is modelled as a cyclic Timoshenko beam that allows bending in the vertical and horizontal directions, and torsion. The technique can consider nonlinearities.

The main characteristics of the cyclic track–train system are developed in Section 2 of the present article. The modal formulation of a cyclic beam is presented in Section 3 of this article. The train–track model is described in Section 4. The present method facilitates the studies of a variety of dynamic problems. The results of some practical problems associated with the ballast characteristics are presented in Section 5.

2. The cyclic train–track model

The cyclic model provides some benefits with respect to the finite track model and classical infinite model. The finite track models need to keep the vehicle on the track and consequently, the time interval of integration must be shorter than the track length divided by the train velocity; moreover the wheelsets keep distance from the extreme ends of the track in order to avoid the interaction with the waves that reflect at the track end; the length of the cyclic model does not depend on the time interval of integration. Infinite track models based on wave propagation techniques and Fourier analysis require adopting linear hypotheses; the cyclic model can consider nonlinear elements.

The cyclic track–train system is an infinite track model on which there are an infinite number of identical vehicles spaced at a regular interval of characteristic distance L (see Fig. 1) and running at identical speed V. The characteristic distance is an arbitrary value selected in such a way that the vehicles are dynamically uncoupled; the waves created in a vehicle must not reach the adjacent vehicles. Without lose of generality, the characteristic distance is chosen as a multiple of the sleeper bay distance L_b.

The analysis can be carried out if an L-length sample of the track is considered (see Fig. 2). The displacements at the ends of the sample rails have to be the same. This boundary condition is considered in the next section in order to obtain the modal properties of the cyclic Timoshenko beam.

The cyclic track can be used for simulating transient phenomena and obtaining a stationary response of the track, in linear or nonlinear models. Vibration modes cannot be considered in infinite tracks which must be studied as a wave propagation problem. Nevertheless, the cyclic track admits a modal approach.

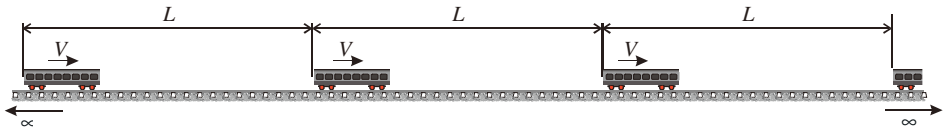

Fig. 1. The cyclic track model.

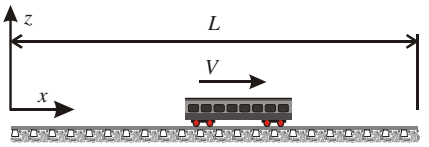

Fig. 2. Characteristic sample of the cyclic track–train system.

3. The cyclic Timoshenko beam

Consider the free vibration of a Timoshenko beam of constant cross-section. Its equations of motion are:

$$-EI\frac{\partial^2\psi}{\partial x^2}+\kappa AG\left(\psi-\frac{\partial w}{\partial x}\right)+mr^2\ddot{\psi}=0, \tag{1}$$

$$\kappa AG\left(\frac{\partial\psi}{\partial x}-\frac{\partial^2 w}{\partial x^2}\right)+m\ddot{w}=0, \tag{2}$$

where $w=w(x,t)$ is the transversal displacement and $\psi=\psi(x,t)$ is the beam section rotation; E is the Young's modulus, I is the second moment of area, A is the cross-sectional area, κ is the Timoshenko shear coefficient, m is the linear mass density and G is the shear modulus. The solution has the following form:

$$w(x,t)=W(x)q(t), \tag{3}$$

$$\psi(x,t)=\Psi(x)q(t). \tag{4}$$

If a harmonic solution of the free response is accepted, then $q(t)=\overline{q}e^{i\omega t}$. Eqs. (1) and (2) then become

$$-EI\frac{\partial^2\Psi}{\partial x^2}+\kappa AG\left(\Psi-\frac{\partial W}{\partial x}\right)-\omega^2 mr^2\Psi=0, \tag{5}$$

$$\kappa AG\left(\frac{\partial\Psi}{\partial x}-\frac{\partial^2 W}{\partial x^2}\right)-\omega^2 mW=0. \tag{6}$$

Eq. (6) is differentiated with respect to x and the resultant equation in Ψ is substituted into (5). This yields

$$\Psi=\frac{1}{\kappa AG-\omega^2 mr^2}\left(\left(EI\frac{\omega^2 m}{\kappa AG}+\kappa AG\right)\frac{\partial W}{\partial x}+EI\frac{\partial^3 W}{\partial x^3}\right). \tag{7}$$

Eq. (7) can be substituted into Eqs. (5) and (6), and by combining them the following equation of motion is obtained:

$$EI\frac{\partial^4 W}{\partial x^4}+\left(EI\frac{\omega^2 m}{\kappa AG}+\omega^2 mr^2\right)\frac{\partial^2 W}{\partial x^2}-\left(\omega^2 m-\frac{\omega^4 m^2 r^2}{\kappa AG}\right)W=0. \tag{8}$$

The mode shape $W(x)$ is the well-known formula:

$$W(x)=A\sin\frac{\lambda x}{L}+B\cos\frac{\lambda x}{L}+C\sinh\frac{\chi x}{L}+D\cosh\frac{\chi x}{L}. \tag{9}$$

In order to verify the boundary conditions (cyclic structure), the following restrictions must be satisfied:

$$W(0)=W(L), \tag{10}$$

$$W^{(j)}(0)=W^{(j)}(L),\quad j=1,2,\ldots,\infty, \tag{11}$$

where the superscript (j) refers to the jth derivative. The boundary conditions expressed in Eqs. (10) and (11) can only be fulfilled if constants C and D of Eq. (9) are zero. The corresponding characteristic equation produces

$$\lambda_n=2\pi n,\quad n=0,1,\ldots,\infty, \tag{12}$$

which has multiplicity of 2. The corresponding modal functions are:

$$W_{2n-1}=A_n\sin\frac{\lambda_n x}{L}, \tag{13}$$

and

$$W_{2n}=B_n\cos\frac{\lambda_n x}{L}. \tag{14}$$

The index n=0 has been selected for rigid-body modes. Rotations are obtained from the transverse displacements through Eq. (7), and they are

$$\Psi_{2n-1} = \frac{A_n}{\kappa AG - \omega_n^2 mr^2}\left(\left(EI\frac{\omega_n^2 m}{\kappa AG} + \kappa AG\right)\frac{\lambda_n}{L} - EI\frac{\lambda_n^3}{L^3}\right)\cos\frac{\lambda_n x}{L} \tag{15}$$

and

$$\Psi_{2n} = \frac{B_n}{\kappa AG - \omega_n^2 mr^2}\left(-\left(EI\frac{\omega_n^2 m}{\kappa AG} + \kappa AG\right)\frac{\lambda_n}{L} + EI\frac{\lambda_n^3}{L^3}\right)\sin\frac{\lambda_n x}{L}. \tag{16}$$

Any of the eigenfunctions, (13) or (14) can be substituted into (8) and the following algebraic equation is found:

$$\frac{m^2 r^2 L^4}{\kappa AG}\omega_n^4 - \left(\frac{EI\lambda_n^2 L^2 m}{\kappa AG} + mr^2\lambda_n^2 L^2 + mL^4\right)\omega_n^2 + EI\lambda_n^4 = 0. \tag{17}$$

Two families of natural frequencies are found. They are:

$$\widehat{\omega}_n = \sqrt{\frac{\left(EI\lambda_n^2 L^2 m + \left(mr^2\lambda_n^2 L^2 + mL^4\right)\kappa AG\right) - \sqrt{\left(EI\lambda_n^2 L^2 m + \left(mr^2\lambda_n^2 L^2 + mL^4\right)\kappa AG\right)^2 - 4m^2 r^2 L^4 EI\lambda_n^4}}{2m^2 r^2 L^4}}, \tag{18}$$

$$\breve{\omega}_n = \sqrt{\frac{\left(EI\lambda_n^2 L^2 m + \left(mr^2\lambda_n^2 L^2 + mL^4\right)\kappa AG\right) + \sqrt{\left(EI\lambda_n^2 L^2 m + \left(mr^2\lambda_n^2 L^2 + mL^4\right)\kappa AG\right)^2 - 4m^2 r^2 L^4 EI\lambda_n^4}}{2m^2 r^2 L^4}}. \tag{19}$$

Each mode family is formed by a set of four eigenfunctions and a natural frequency. For the first family, they are $\widehat{W}_{2n-1}$, $\widehat{W}_{2n}$, $\widehat{\Psi}_{2n-1}$, $\widehat{\Psi}_{2n}$ and $\widehat{\omega}_n$; for the second one, $\breve{W}_{2n-1}$, $\breve{W}_{2n}$, $\breve{\Psi}_{2n-}1$, $\breve{\Psi}_{2n}$ and $\breve{\omega}_n$. Those researchers familiar with Euler beam (where each mode is defined just through the transversal displacement) must consider that $\widehat{W}_j$ and $\breve{W}_j$ can be the same function, but they are associated with different modes because $\widehat{\Psi}_j$ and $\breve{\Psi}_j$ are different. It can be shown in Fig. 3 where the first mode of each family is plotted. In this case, the first mode of the first family is similar to the corresponding Euler mode. Nevertheless, in the second family the transversal modal displacements are relatively small, and the mode mainly consists of rotations of the beam's cross-sections.

The mass normalisation of mode shapes

$$\int_0^L \left(mW^2 + mr^2\Psi^2\right)\mathrm{d}x = 1, \tag{20}$$

leads to

$$B_n = \frac{\sqrt{2mL\left(1 + D_n^2 r^2\right)}}{mL\left(1 + D_n^2 r^2\right)}, \tag{21}$$

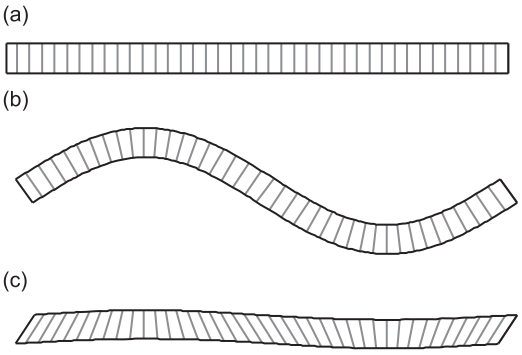

Fig. 3. The Timoshenko cyclic beam and its first deformed shapes. The grey lines show the cross-section of the beam: (a) undeformed beam, (b) first mode $\widehat{W}_1$ of the first family set and (c) first mode $\breve{W}_2$ of the second family set.

where

$$D_n = \frac{1}{\kappa AG - \omega_n^2 m r^2}\left(-\left(EI\frac{\omega_n^2 m}{\kappa AG} + \kappa AG\right)\frac{\lambda_n}{L} + EI\frac{\lambda_n^3}{L^3}\right). \tag{22}$$

It can be easily proved that $A_n = B_n$.

4. Proposed model

The dynamic model employs a substructuring technique. The whole system consists of the following substructures: rails, the vehicle and the under-rail substructures. In the present work the under-rail substructures are the sleepers. The equations of motion of each substructure are considered separately, and the whole system is brought together through the forces at the wheel/rail contact and the railpad. The vehicle equations of motion are expressed in a set of physical coordinates, corresponding to a lumped parameters model. The rail is a cyclic Timoshenko beam and is described by a modal approach for the reason stated in Section 1. The modal approach is also adopted for the under-rail substructures. This method provides the same mathematical expressions of the equation of motion independently of the studied substructure (sleeper, bridge, ground, etc.), and consequently the flexibility of the technique is guaranteed. It is illustrated in Fig. 4.

The forces in the railpad are functions of the displacements and velocities of the rail and the sleeper at the railpad position. The forces at the wheel/rail contact are functions of the displacements and velocities of the rail and the wheel at the contact patch.

Each substructure employs a local coordinate frame. However, a global coordinate frame *xyz* is also defined with the positive *x*-axis parallel to the rail in the direction of vehicle motion, the *y*-axis transverse to the track and the vertical *z*-axis positive upwards.

4.1. Rail dynamics

The lateral, vertical and torsional vibrations of the rail are coupled through the wheel/rail contact and the railpad forces. The lateral and vertical displacements of the rail axis are:

$$w^y(x,t) = \sum_r W_r^y(x) q_r^y(t), \tag{23}$$

$$w^z(x,t) = \sum_r W_r^z(x) q_r^z(t) \tag{24}$$

and the torsion and the rotations of the rail's cross-section are:

$$\psi^x(x,t) = \sum_r \Psi_r^x(x) q_r^x(t), \tag{25}$$

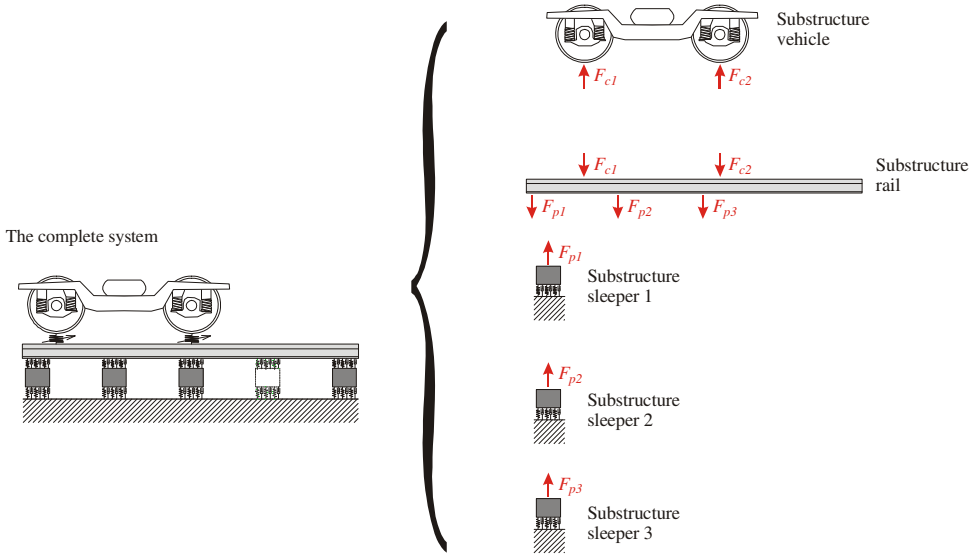

Fig. 4. The substructuring technique for a standard track.

$$\psi^y(x,t)=\sum_r \Psi_r^y(x)q_r^z(t), \tag{26}$$

$$\psi^z(x,t)=\sum_r \Psi_r^z(x)q_r^y(t). \tag{27}$$

where $W_r^y(x)$, $W_r^z(x)$, $\Psi_r^x(x)$, $\Psi_r^y(x)$ and $\Psi_r^z(x)$ are the rth modal functions of the Timoshenko periodic beam, and $q_r^x(t)$, $q_r^y(t)$ and $q_r^z(t)$ are the modal coordinates associated with torsional, lateral and vertical rail vibrations, respectively.

The equation of motion of the rails in modal coordinates is (note that the superscript associated with the dynamic type has been intentionally omitted)

$$\ddot{q}_r+2\xi_r\omega_r\dot{q}_r+\omega_r^2q_r=f_r, \tag{28}$$

where ω_r is the rth undamped frequency and ξ_r is the modal damping. The modal forces f_r are computed from the force set F_i and torque set T_j through the shape functions computed at the point where the force is applied.

4.2. Under-rail substructure dynamics

In most cases, the under-rail substructures are the sleepers. Each sleeper is implemented through a modal approach. The equation of motion resembles Eq. (28). The modal properties of the substructure are computed from an FE model of the sleeper. The method is capable of accommodating more complex substructures. For example, if all the sleepers are elastically coupled (see Fig. 5) they would form a single substructure governed by Eq. (28).

4.3. Vehicle dynamics

A vehicle in general possesses viscous damping and/or gyroscopic damping [23,24] and rarely its equations of motion can be decoupled. The general form of the equations of motion for the vehicle can be written as

$$\mathbf{M}\ddot{\mathbf{x}}+\mathbf{C}\dot{\mathbf{x}}+\mathbf{K}\mathbf{x}=\mathbf{F}_{ext}, \tag{29}$$

where $\mathbf{M}$, $\mathbf{C}$ and $\mathbf{K}$ are the mass, viscous/gyroscopic damping and stiffness matrices of the vehicle, and $\mathbf{F}_{ext}$ is the vector of external forces (such as gravity loads and the wheel–rail contact forces).

4.4. Railpad forces

The railpad forces are functions of the displacements of the sleeper and the rail at the railpad position. The simplest railpad model is a linear one, where the forces are expressed as follows:

$$\overline{\mathbf{F}}_p=\mathbf{K}_p(\mathbf{u}_r^p-\mathbf{u}_s^p), \tag{30}$$

where $\mathbf{K}_p$ is a 6×6 stiffness matrix, and $\mathbf{u}_r^p$ and $\mathbf{u}_s^p$ are the vector of rail and sleeper displacements ($\mathbf{u}_r^p$ and $\mathbf{u}_s^p$ include 3 translations and 3 rotations).

The displacements of the rail at the pad are computed from the rail displacement at the rail axis (Fig. 6) as follows

$$\mathbf{u}_r^p=\mathbf{T}\left\{\begin{array}{ccccc} w^y & w^z & \psi^x & \psi^y & \psi^z \end{array}\right\}^{\mathrm{T}}, \tag{31}$$

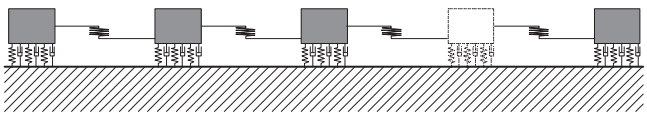

Fig. 5. Elastic coupling in the sleepers.

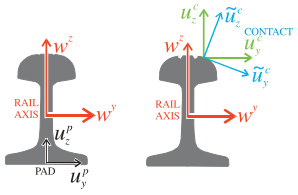

Fig. 6. Displacements at the rail section.

where

$$\mathbf{T}=\begin{bmatrix}0 & 0 & 0 & z & 0\\ 1 & 0 & -z & 0 & 0\\ 0 & 1 & 0 & 0 & 0\\ 0 & 0 & 1 & 0 & 0\\ 0 & 0 & 0 & 1 & 0\\ 0 & 0 & 0 & 0 & 1\end{bmatrix} \tag{32}$$

and z is the distance between the rail axis and the point of the rail section where the force is applied. The last transformation matrix is also employed for obtaining the force at the rail axis

$$\mathbf{F}_p=-\mathbf{T}^{\mathrm{T}}\overline{\mathbf{F}}_p. \tag{33}$$

In the present work, a viscoelastic force model has been implemented.

4.5. Wheel–rail contact forces

The basic and the advanced wheel–rail contact theories can be found in Kalker's monograph in [26]. The present method adopts Hertz's theory for solving the normal contact problem and FASTSIM for the tangential contact problem. Hertz's theory leads to an elliptical contact area and a normal force as a function of the approach. The approach or the penetration of the undeformed solids is obtained from the displacements of the rail and the wheel at the contact patch and the irregularities of the wheel tread and the rail. The contact problem is analysed in a local contact frame where two axes are tangential to the surfaces of the wheel and rail at the contact point (see Fig. 6). The displacements and velocities of the rail at the contact point in local coordinates are the following:

$$\mathbf{u}_r^c=\mathbf{RT}\left\{\begin{array}{ccccc} w^y & w^z & \psi^x & \psi^y & \psi^z\end{array}\right\}^{\mathrm{T}}, \tag{34}$$

$$\dot{\mathbf{u}}_r^c=\mathbf{RT}\left\{\begin{array}{ccccc} \dot{w}^y & \dot{w}^z & \dot{\psi}^x & \dot{\psi}^y & \dot{\psi}^z\end{array}\right\}^{\mathrm{T}}+V\mathbf{RT}\frac{\partial}{\partial x}\left\{\begin{array}{ccccc} w^y & w^z & \psi^x & \psi^y & \psi^z\end{array}\right\}^{\mathrm{T}}, \tag{35}$$

where $\mathbf{R}$ is a rotation matrix.

In high-frequency dynamics, the wheels are supposed to be cylinders and the real profiles are neglected. Consequently, the contact is produced on the top of the rail head and the local and global frames are parallel. The normal force is obtained from the Hertz model as

$$F_c=K_H\delta^{1.5}, \tag{36}$$

where K_H depends on the mechanical properties of the wheel and rail materials and the geometry of the wheel and rail at the contact point, and δ is the approach. The reduced creep velocities in the longitudinal and lateral direction are:

$$\zeta_x=\frac{v^x_{\mathrm{wheel}}-\mathbf{i}\cdot\dot{\mathbf{u}}_r^c}{V}, \tag{37}$$

$$\zeta_y=\frac{v^y_{\mathrm{wheel}}-\mathbf{j}\cdot\dot{\mathbf{u}}_r^c}{V}, \tag{38}$$

being $\mathbf{i}$ and $\mathbf{j}$ the unit vectors along the x and y axes, v^x_{wheel} and v^y_{wheel} the velocities in the x- and y-direction of the wheel at the contact point.

5. Application to hanging sleepers and ballast compaction force

This section presents results from the dynamic model applied to a number of situations. The calculations are aimed at investigating certain engineering problems associated with ballast conditions. They are the presence of a hanging or unsupported sleeper and the ballast compaction types. Both cases concern the maintenance operations through tamping. The dynamics in the presence of a hanging sleeper was studied in [22] through an FE model; different cases of ballast compaction under the sleeper were described in [23]. A hanging sleeper accelerates ballast degradation; a severe case produces broken ballast stones around the unsupported sleeper that can be detected by means of a visual inspection. A correct ballast compaction is key to ensure the appropriate track geometry. Inadequate compaction will lead to the development of track twist, this in turn inducing torsional stresses in the rails.

The simulation data has been taken from [24] where the sleeper is considered rigid. The bay distance is 60 cm, the axle load is 200 kN and the track and the wheel have no irregularities. In the simulations, 100 vertical, lateral and torsional modes of the rails were adopted; 60 sleeper bays were considered. The resultant number of degrees of freedom was big and can be reduced without lose of precision through the method proposed in [21]. The suitable track length depends on the track parameters (that affect the rate of decay of vibration with distance, such as viscous-elastic properties of railpad and

ballast, rail stiffness), the loading and contact conditions (such as corrugation, wheelflat impact), and so on. The number of sleeper bays employed in published finite-length models differed significantly. For example, the simulations carried out in [3] adopted 5 sleeper bays; reference [22] developed a 29-sleeper bay track; while 70 sleeper bays were included in [19]. The error associated with the track length can be estimated when compared with the results of an oversized model. An example of this analysis is presented in Appendix A of this article.

The first result is presented in Fig. 7, which shows the vertical wheel–rail contact force responses when the vehicle is running over a hanging sleeper. The calculations were carried out for four different gap sizes. The vertical dashed lines plot the instant when the wheel is on a sleeper. The vehicle speed is 144 km/h. The time $t=0$ corresponds to the instant when the wheel is over the hanging sleeper.

The results did not show high contact forces as in the case of a wheelflat. However, the amplitude of the wheel–rail contact force should be higher if the gap and the velocity are increased. The latter case is shown in Fig. 8, where the maximal and minimal peak contact forces versus vehicle speed are plotted. The maximum peak force in the studied case is a monotonically increasing function of the vehicle speed. However the hanging sleeper may stay unsupported (it is not in contact with the ballast) during the vehicle passage if the gap is big enough. Fig. 9 shows the maximal and minimal vertical wheel–rail contact forces at different hanging sleeper gap sizes. The calculations were carried out at 144 km/h vehicle speed. It can be seen that at above 1.8 mm gap size the forces do not vary with the gap size.

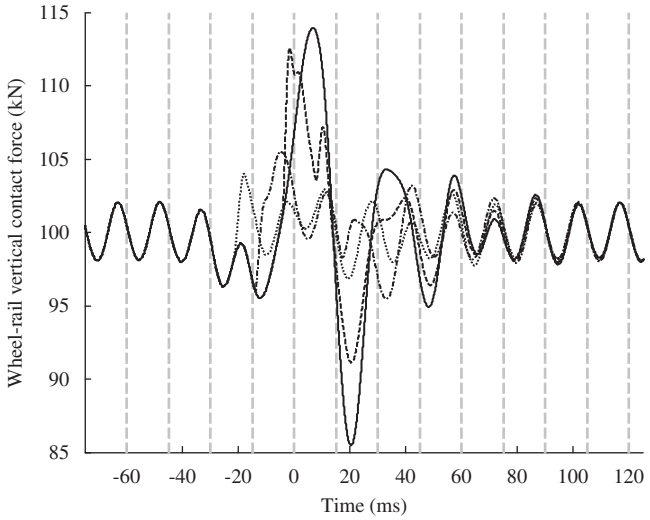

Fig. 7. Wheel–rail vertical contact force due to a hanging sleeper for several gap sizes (· · · · · · , 0.52 mm; -·-·-·-, 0.95 mm; ——, 1.47 mm; ——, 2 mm). The vertical dashed lines plot the instant when the wheel is on a sleeper. The wheel passes over the unsupported sleeper at time $t=0$. Vehicle speed 144 km/h.

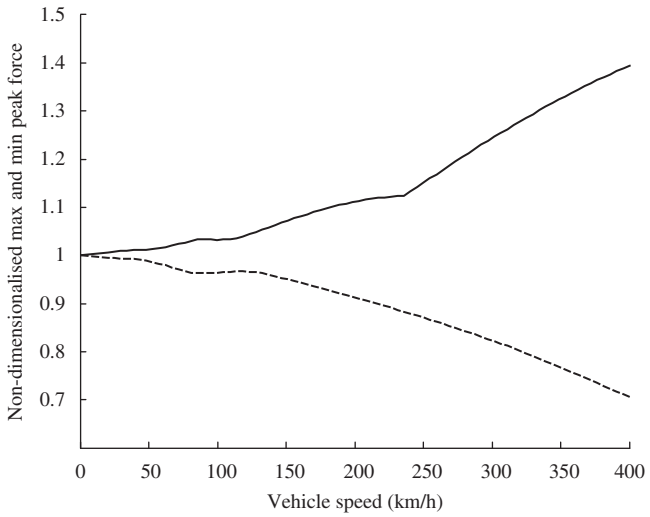

Fig. 8. Maximal (——) and minimal (——) wheel–rail contact forces due to a hanging sleeper (1 mm gap) at different vehicle speeds. The forces were normalised with respect to the static load.

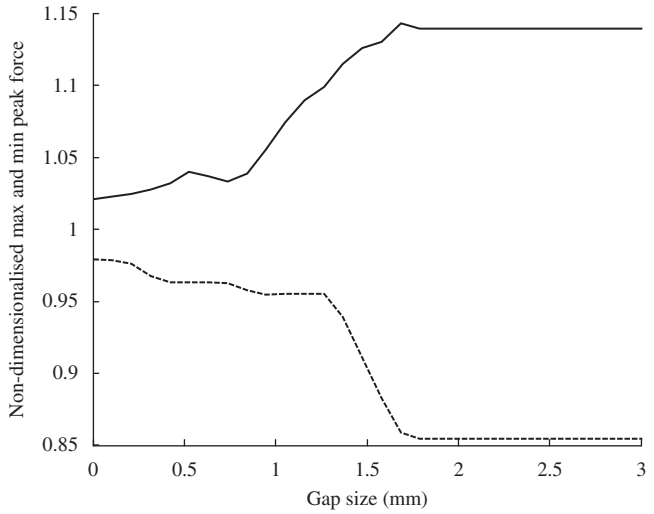

Fig. 9. Maximal (——) and minimal (– –) wheel–rail contact forces for different hanging sleeper gap sizes. The forces were normalised with respect to the static load. Vehicle speed 144 km/h.

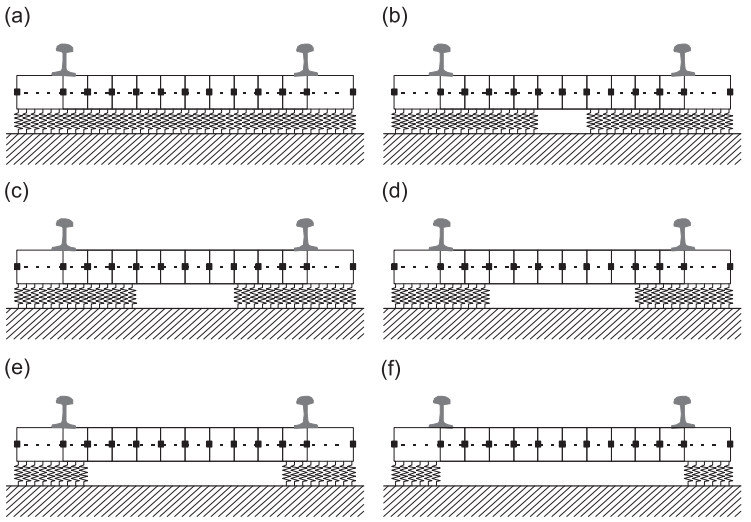

Fig. 10. Sleeper models: (a) the ballast is uniform under the sleeper and (b–f) the ballast is progressively offset towards the sleeper edges. The total foundation stiffnesses are identical in all the cases.

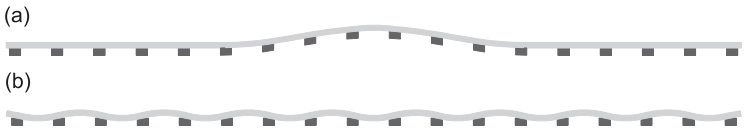

Fig. 11. Mode shapes of the railway track. (a) The P2 mode, where rails and sleepers are bouncing on ballast stiffness. (b) The pinned–pinned mode, which is a bending mode of the rail with the sleepers giving rise to nodes and the sleeper spacing corresponding to half a wavelength.

In order to study different cases of ballast compaction, the following calculations implement a flexible model of the sleeper. Fig. 10 shows the sleeper ballast distribution types. In order to keep the P2 resonance (or loaded track resonance, see Fig. 11) approximately constant, the total ballast stiffness is assumed to be 100 MN/m in all the cases. The modal properties of the sleeper needed in the modal approach are obtained from a FE beam model of the sleeper, which contains 12 elements (Timoshenko beam or Timoshenko beam on a Winkler foundation).

Fig. 12 presents the bending moment responses that were computed for different sleeper types (the types were presented in Fig. 10). The time $t=0$ corresponds to the instant when the wheel is over the sleeper involved. The differences were considerable and they suggest that sleepers should be in contact with the rails.

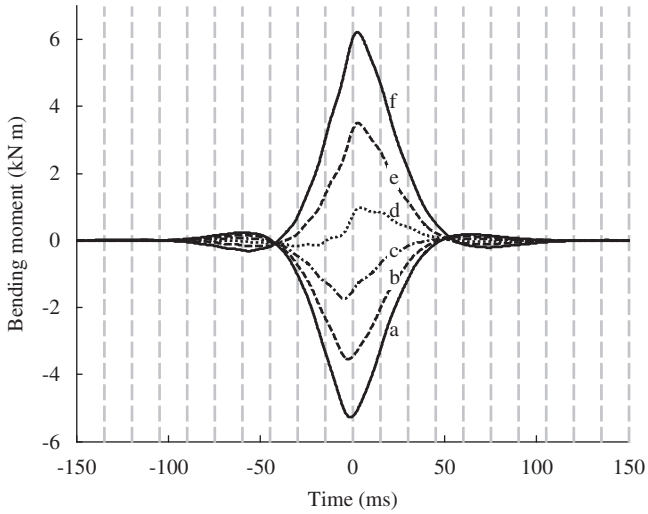

Fig. 12. Bending moment response at the middle of the sleeper for various different cases of ballast compaction. The notation (a–f) is in accordance with Fig. 10. The vertical dashed lines plot the instant when the wheel is on a sleeper. The wheel comes over the analysed sleeper at time t=0.

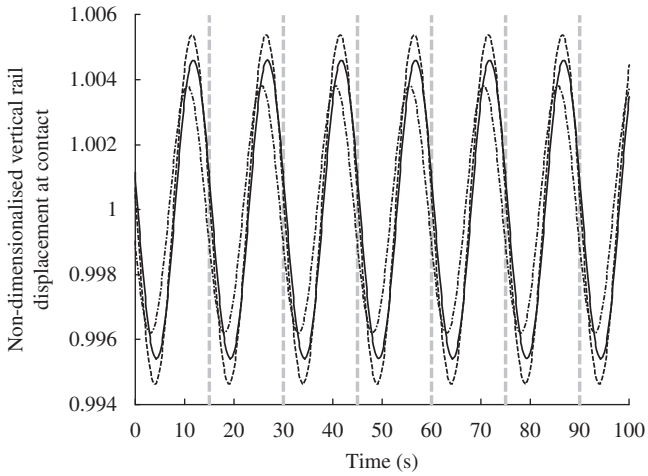

Fig. 13. Non-dimensionalised vertical displacement of the rail at the contact point for the sleeper models (——, ballast compaction type a; ——, ballast compaction type d; ——, ballast compaction type f). The vertical dashed lines plot the instant when the wheel is on a sleeper.

The track stiffness depends slightly on the ballast distribution because of the bending stiffness of the sleeper. Sleeper types a and f (notation in accordance with Fig. 10) are slightly softer than types b, c, d and e (the average of the static displacement for the sleeper types a, d and f are -0.99, -0.97 and -1.20 mm, respectively). The rail displacements associated with different sleeper types are non-dimensionalised with respect to the static displacement in order to compare the dynamic responses. Fig. 13 presents the non-dimensionalised vertical displacements of the rail at the contact point. Their amplitudes are mainly influenced by the track stiffness because the frequency is low when compared with the track frequencies.

Fig. 14 presents the vertical force versus the total tangential contact force. This is the stationary response and it was computed for different sleeper types. This plot provides rough information about the wear mechanisms and the general vehicle–track interaction behaviour. The differences among the forces obtained for various sleeper types are due to stiffness variation and are seen to be small.

6. Conclusions

The present work developed a new methodology for modelling the coupled dynamics of a railway vehicle and the track. The technique considered an infinite cyclic train–track system, on which an infinite set of identical railway vehicles were running. This reasonable simplification led to fairly realistic results and at the same time could accommodate nonlinearities such as a gap at the sleeper support or in the wheel–rail contact force model. The modal approach permitted

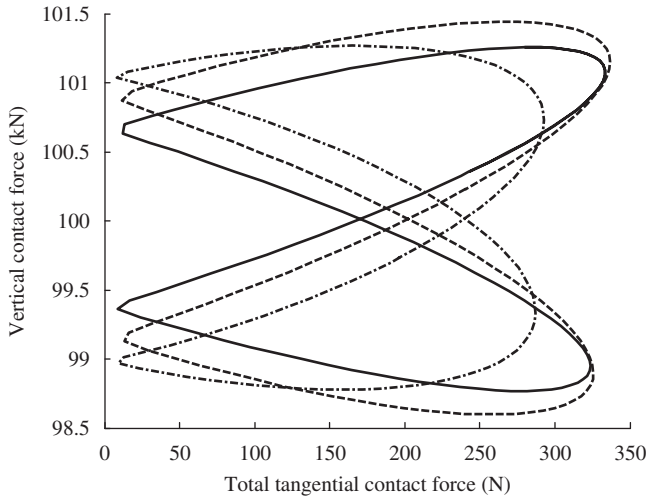

Fig. 14. Vertical contact force vs. total tangential contact force plot for the sleeper models (——, ballast compaction type a; ——, ballast compaction type d; ——, ballast compaction type f).

simulations through a reduced number of coordinates, which produced a non-stiff ordinary differential equation system that can be integrated with a reduced computational cost. The cyclic track assumption allows simulations for an unlimited time period.

The method was first applied to analyse the dynamic response in the presence of a hanging sleeper; and secondly, to study different cases of ballast compaction under the sleeper. The numerical results of the first analysis show that the wheel–rail contact force amplitude is big at high velocities and there is an innocuous gap size above which similar low responses are produced. However, it must be highlighted that the effect of velocity is more remarkable. The ballast compaction types produced a notable effect on the bending moment at the sleeper. Nevertheless the influence of the sleeper model on the dynamic behaviour of the vehicle–track system was found to be small.

Acknowledgements

The first author gratefully acknowledges the support for this work provided by the Project TRA2010-15669 (Ministerio de Ciencia e Innovación).

Appendix A

This section describes a method for obtaining the suitable characteristic length L of the track model. To this end, the error associated with the track length can be estimated when compared with the results of an oversized model.

The rate of decay of vibration with distance is lower at the pinned–pinned frequency (see Fig. 11) because this frequency is associated with the less damped mode. Consequently the most unfavourable case that needs a higher characteristic length corresponds to a vehicle running on a track where the rail roughness excites the pinned–pinned mode. The pinned–pinned frequency can be derived from Eq. (18), and that is

$$\omega_{pp}=\sqrt{\frac{(4EI\pi^2L_b^2m+4(mr^2\pi^2L_b^2+mL_b^4)\kappa AG)-\sqrt{(EI\pi^2L_b^2m+(mr^2\pi^2L_b^2+mL_b^4)\kappa AG)^2-64m^2r^2L_b^4EI\pi^4}}{16m^2r^2L_b^4}}. \tag{A.1}$$

For the rail parameters that are used in Section 5, this frequency is 1069.0 Hz. If the vehicle velocity is 40 m/s, the roughness wavelength that matches the wavelength of the pinned–pinned frequency is 37.4 mm. The ISO 3095 standard provides the limit of rail roughness that is adopted in the present analysis; at 44 mm wavelength, it corresponds to harmonic roughness amplitude of 1.66 μm. These parameters are used in the present simulations.

Fig. A1 shows the vertical contact force due to a harmonic roughness that is resonant with the pinned–pinned frequency. The calculations were carried out through different characteristic lengths. This result shows the coherence of the 60 sleeper bays model and the oversized 110 sleeper bays model for this unfavourable case.

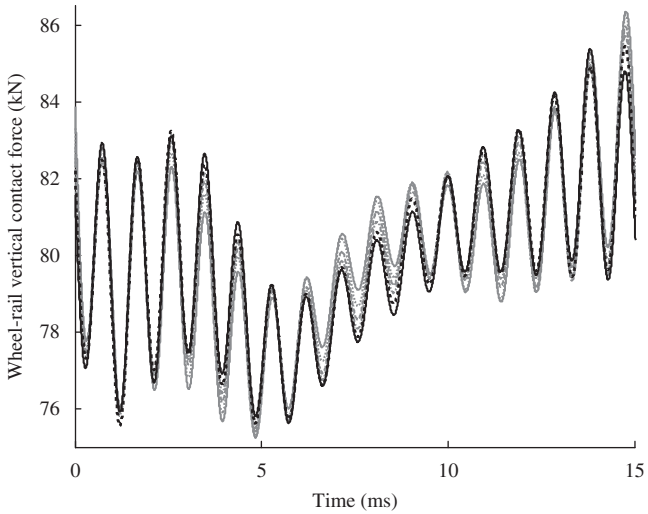

Fig. A1. Vertical contact force responses due to rail corrugation through different characteristic lengths. The corrugation wavelength corresponds to the pinned–pinned frequency at V=40 m/s (——, black, L=66 m, 110 sleeper bays; · · · · · · , black, 60 sleeper bays; - · - · , grey, 40 sleeper bays; — —, grey, 30 sleeper bays; · · · · · · , grey, 20 sleeper bays; ——, grey, 10 sleeper bays).

References

[1] J.C.O. Nielsen, A. Johansson, Out-of-round railway wheels—a literature survey, *Proceedings of the Institution of Mechanical Engineers, Part F: Journal of Rail and Rapid Transit* 214 (2000) 79–91.
[2] S.L. Grassie, Rail corrugation: characteristics, causes, and treatments, *Proceedings of the Institution of Mechanical Engineers, Part F: Journal of Rail and Rapid Transit* 223 (2009) 581–596.
[3] Z. Li, X. Zhao, C. Esveld, R. Dollevoet, M. Molodova, An investigation into the causes of squats—correlation analysis and numerical modelling, *Wear* 265 (2008) 1349–1355.
[4] D. Thompson, *Railway Noise and Vibration: Mechanisms, Modelling and Means of Control*, Elsevier, 2009 ISBN13:978-0-08-045147-3.
[5] L. Jézéquel, Response of periodic system to a moving load, *Journal of Applied Mechanics—ASME* 48 (1981) 613–618.
[6] M. Shamalta, A.V. Metrikine, Analytical study of the dynamic response of an embedded railway track to a moving load, *Archive of Applied Mechanics* 73 (2003) 131–146.
[7] M.F.M. Hussein, H.E.M. Hunt, Modelling of floating-slab tracks with continuous slabs under oscillating moving loads, *Journal of Sound and Vibration* 297 (2006) 37–54.
[8] A.V. Vostroukhov, A.V. Metrikine, Periodically supported beam on a visco-elastic layer as a model for dynamic analysis of a high-speed railway track, *International Journal of Solids and Structures* 40 (2003) 5723–5752.
[9] G. Lombaert, G. Degrande, D. Clouteau, Numerical modelling of free field traffic-induced vibrations, *Soil Dynamics and Earthquake Engineering* 19 (2000) 473–488.
[10] P.M. Belotserkovskiy, On the oscillations of infinite periodic beams subjected to a moving concentrated force, *Journal of Sound and Vibration* 193 (1996) 705–712.
[11] C.W. Cai, Y.K. Cheung, H.C. Chan, Dynamic-response of infinite continuous beams subjected to a moving force—an exact method, *Journal of Sound and Vibration* 123 (1988) 461–472.
[12] D.J. Mead, Free wave propagation in periodically supported infinite beams, *Journal of Sound and Vibration* 11 (1970) 181–197.
[13] D.J. Thompson, Wheel–rail noise generation, part III: rail vibration, *Journal of Sound and Vibration* 161 (1993) 421–446.
[14] L. Gry, C. Gontier, Dynamic modelling of railway track: a periodic model based on a generalized beam formulation, *Journal of Sound and Vibration* 199 (1997) 531–558.
[15] J. Gómez, E. García-Vadillo, J. Santamaría, A comprehensive track model for the improvement of corrugation models, *Journal of Sound and Vibration* 293 (2006) 522–534.
[16] F. Lu, D. Kennedy, F.W. Williams, J.H. Lin, Symplectic analysis of vertical random vibration for coupled vehicle–track systems, *Journal of Sound and Vibration* 317 (2008) 236–249.
[17] R.G. Dong, S. Sankar, R.V. Dukkipati, A finite-element model of railway track and its application to the wheel flat problem, *Proceedings of the Institution of Mechanical Engineers, Part F: Journal of Rail and Rapid Transit* 208 (1994) 61–72.
[18] X. Lei, N.-A. Noda, Analyses of dynamic response of vehicle and track coupling system with random irregularity of track vertical profile, *Journal of Sound and Vibration* 258 (2002) 147–165.
[19] J.C.O. Nielsen, A. Igeland, Vertical dynamic interaction between train and track—influence of wheel and track imperfections, *Journal of Sound and Vibration* 187 (1995) 825–839.
[20] A.A. Shabana, R. Chamorro, C. Rathod, A multi-body system approach for finite-element modelling of rail flexibility in railroad vehicle applications, *Proceedings of the Institution of Mechanical Engineers, Part K: Journal of Multi-body* 222 (2008) 1–15.
[21] L. Baeza, A. Roda, J.C.O. Nielsen, Railway vehicle/track interaction analysis using a modal substructuring approach, *Journal of Sound and Vibration* 293 (2006) 112–124.
[22] A. Lundqvist, T. Dahlberg, Load impact on railway track due to unsupported sleepers, *Proceedings of the Institution of Mechanical Engineers, Part F: Journal of Rail and Rapid Transit* 219 (2005) 67–77.
[23] C. Esveld, *Modern Railway Track*, MRT-Productions90-800324-3-3, 2001.
[24] G. Xie, S.D. Iwnicki, Simulation of wear on a rough rail using a time-domain wheel–track interaction model, *Wear* 265 (2008) 1572–1583.